

Distorted wave Born approximation fit to  $^{13}\text{C}(d,p)^{14}\text{C}$  cross section data at  $E_d=200\text{--}350$  keVA. A. Naqvi,<sup>1,\*</sup> M. M. Nagadi,<sup>2</sup> S. Kidwai,<sup>2</sup> and Khateeb-ur-Rehman<sup>2</sup><sup>1</sup>Center for Applied Physical Sciences, King Fahd University of Petroleum and Minerals, Dhahran 31261, Saudi Arabia<sup>2</sup>Physics Department, King Fahd University of Petroleum and Minerals, Dhahran 31261, Saudi Arabia

(Received 20 April 2001; published 9 May 2002)

Angular distributions of the differential cross section for the  $^{13}\text{C}(d,p)^{14}\text{C}$  reaction at 200–350 keV deuteron energies have been calculated using the finite range distorted wave Born approximation (DWBA) model and have been compared with the experimental data. Optical model parameters data used in the present DWBA model calculations, was taken from previous normalized zero-range DWBA calculations for the  $^{13}\text{C}(d,p)^{14}\text{C}$  reaction at 410–810 keV deuteron energies. There is good agreement between the finite range DWBA model calculations and the experimental  $^{13}\text{C}(d,p)^{14}\text{C}$  cross section data at 200–350 keV deuteron energies. For the sake of comparison, the angular distributions were also calculated using the zero-range DWBA approximation. It was observed that the differential cross section obtained from normalized zero-range calculations over 200–350 keV deuteron energies was about 30–40 % smaller than that obtained from finite range calculations. The study has shown that the  $^{13}\text{C}(d,p)^{14}\text{C}$  reaction at such low deuteron energies still proceed through the direct reaction channel and can be explained using the finite-range DWBA model.

DOI: 10.1103/PhysRevC.65.054615

PACS number(s): 25.45.Hi, 25.40.Hs

## I. INTRODUCTION

Deuteron stripping reactions are highly selective and strongly populate states in the residual nucleus by simply adding a neutron to the ground state of the target nucleus [1–5]. The distorted wave Born approximation (DWBA) model has been successfully used in predicting the correct cross section for deuteron stripping reactions using zero-range as well as finite-range approximations [2–5]. Although the zero-range approximation is inaccurate in treating the contributions from reactions occurring inside the nucleus [4], it has been successfully used to predict cross section for high  $Q$ -value ( $d, p$ ) reactions where DWBA calculations are sensitive to the interior wave function of the projectile. Generally this is done using normalized zero-range DWBA calculations [2] where normalization factor for such calculations depends upon the reaction kinematics. An exact treatment of such reactions can be obtained using finite-range DWBA calculations.

Previously cross section data of low as well as high  $Q$ -valued reactions such as  $^{12}\text{C}(d,p)^{13}\text{C}$ ,  $^{13}\text{C}(d,p)^{14}\text{C}$ ,  $^{13}\text{C}(d,t)^{12}\text{C}$ , and  $^{13}\text{C}(d,\alpha_0,1)^{11}\text{B}$  at  $E_d=410\text{--}810$  keV have been analyzed using normalized zero-range DWBA approximation [2]. Although there was a good agreement between the normalized zero-range DWBA calculations and experimental cross section data of  $^{12}\text{C}(d,p)^{13}\text{C}$  and  $^{13}\text{C}(d,p)^{14}\text{C}$  reactions but the normalized zero-range DWBA calculations did not produce a good fit to experimental cross section data of  $^{13}\text{C}(d,t)^{12}\text{C}$  and  $^{13}\text{C}(d,\alpha_0,1)^{11}\text{B}$  reactions [2]. It is known that normalized zero-range DWBA calculations predict ( $d, p$ ) cross section nearly identical to those of an exact finite range calculations [2]. In order to verify this fact and investigate the reported discrepancy in Ref. [2], it was worthwhile to measure cross section data at or near the deuteron energies of

Ref. [2] and fit it with finite range DWBA model calculations.

A study has been undertaken at the 350 keV accelerator of King Fahd University of Petroleum and Minerals, Dhahran, Saudi Arabia in which an experimental cross section of  $^{13}\text{C}(d,p)^{14}\text{C}$  cross sections were measured over 200–350 keV deuteron energies [1] to investigate the reported disagreement [2]. In the present study  $^{13}\text{C}(d,p)^{14}\text{C}$  cross section data [1] has been fitted with finite range DWBA calculations. Results of DWBA fit to  $^{13}\text{C}(d,p)^{14}\text{C}$  cross section data are presented in this paper.

II. ANGULAR DISTRIBUTIONS OF THE  $^{13}\text{C}(d,p)^{14}\text{C}$  REACTION

The experimental setup and procedure used to measure the cross section of the  $^{13}\text{C}(d,p)^{14}\text{C}$  reaction has been published in detail elsewhere [1,6,7]. For the sake of continuity, it will be described briefly here. The differential cross section of  $^{13}\text{C}(d,p)^{14}\text{C}$  was measured at the scattering chamber of the 80° beam line of the 350 kV accelerator [8]. Prior to the measurements, the beam energy of the accelerator was calibrated using 224 and 340 keV resonance of the

TABLE I. Experimental and calculated total cross sections of the  $^{13}\text{C}(d,p)^{14}\text{C}$  reaction.

$E_d$ (keV)	$\sigma_{\text{exp}}$ ( $\mu\text{b}$ )	$\sigma_{\text{calc}}(\mu\text{b})$ using		$\sigma_{\text{calc}}(\mu\text{b})$ using	
		$V=79.5$ MeV	$\chi^2$	$V=80.0$ MeV	$\chi^2$
350	$453 \pm 25$	448.1	10	433.4	7
335	$328 \pm 21$	343.7	11	332.2	8
310	$200 \pm 16$	211.1	7	203.9	5
290	$140 \pm 14$	136.3	5	131.5	4
270	$87 \pm 10$	83.6	5	80.6	4
250	$50 \pm 9$	48.2	4	46.5	3
200	$8 \pm 4$	8.4	2	8.1	2

\*Corresponding author.

TABLE II. Optical model parameters used in the present study. They were taken from Ref. [2].

OMP parameters	Entrance channel	Exit channel
$V$ (MeV)	79.50	51.50
$r$ (fm)	1.25	1.30
$a$ (fm)	0.80	0.34
$W$ (MeV)	10.00	19.20
$r_w$ (fm)	1.25	1.30
$a_w$ (fm)	0.80	0.125
$V_{so}$ (MeV)	6.00	6.00
$r_{so}$ (fm)	1.25	1.30
$a_{so}$ (fm)	0.80	0.34
$r_c$ (fm)	1.25	1.25

$^{19}\text{F}(p, \alpha\gamma)^{16}\text{O}$  nuclear reaction. The cross sections were measured using eight silicon surface barrier detectors, each with  $300\ \mu\text{m}$  thickness and  $100\ \text{mm}^2$  effective area. In this study  $30\ \mu\text{g}/\text{cm}^2$  thick enriched  $^{13}\text{C}$  foils were used as targets. The foils were supplied by the Atomic Energy of Canada Limited, Chalk River, Canada. For the deuteron beam flux calculation, the beam transmitted through the target foil was measured at an electrically suppressed Faraday

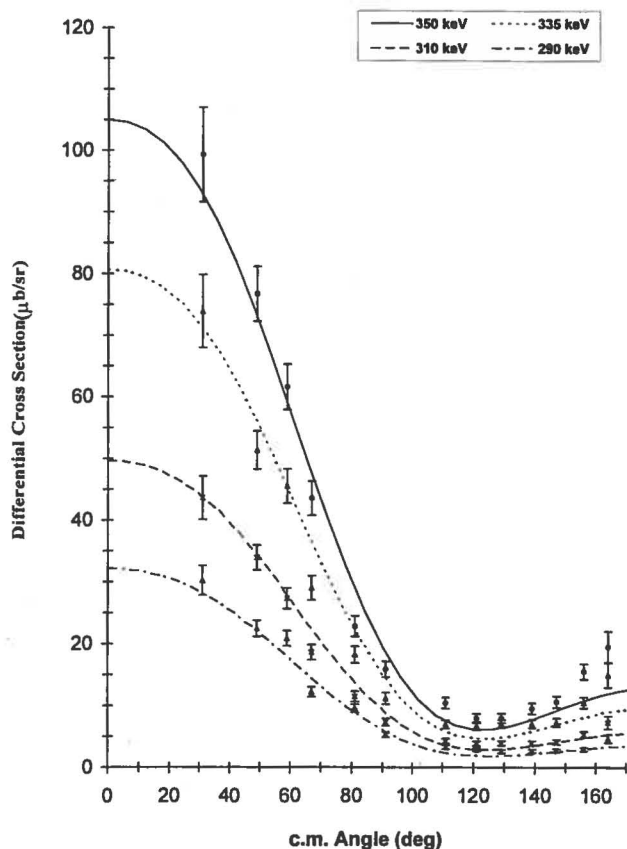


FIG. 1. Angular distributions of the differential cross section for the  $^{13}\text{C}(d,p)^{14}\text{C}$  reaction at 290–350 keV deuteron energies. The dashed and solid curves are the results of the finite range DWBA calculations.

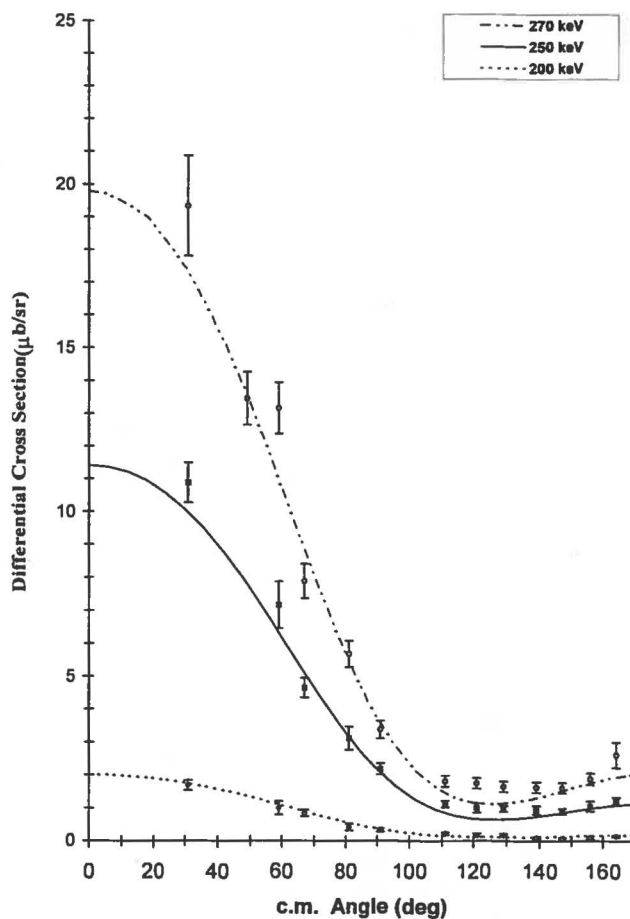


FIG. 2. Angular distributions of differential cross section for the  $^{13}\text{C}(d,p)^{14}\text{C}$  reaction at 200–270 keV deuteron energies. The dashed and solid curves are the results of the finite range DWBA calculations.

cup and was integrated using an electronics module.

The excitation functions of the  $^{13}\text{C}(d,p)^{14}\text{C}$  reaction were measured over 200–350 keV deuteron energies in 10 keV steps at eight angles, namely,  $30^\circ$ ,  $48^\circ$ ,  $66^\circ$ ,  $90^\circ$ ,  $110^\circ$ ,  $128^\circ$ ,  $146^\circ$ , and  $164^\circ$ . The statistical uncertainties in excitation functions were 2 to 6%. The excitation functions are structureless and have a smooth increasing trend with deuteron energy. The angular distributions of the  $^{13}\text{C}(d,p)^{14}\text{C}$  reaction were measured at 200, 250, 270, 290, 310, 335, and 350 keV deuteron energies. The angular distributions are forward peaked with a minimum cross section around  $120^\circ$ . For all angular distributions, the cross section at  $30^\circ$  is almost 10 times larger than that at about  $120^\circ$ – $130^\circ$ . Within statistical uncertainties, all the angular distributions showed a smooth trend and had no structure. The total uncertainties in angular distributions above 250 keV energy varied from 6 to 10% while below 250 keV they were 10 to 30%. The shape of the excitation functions and angular distributions measured in the present work are consistent with the data of Putt [2].

The total cross section of the  $^{13}\text{C}(d,p)^{14}\text{C}$  reaction was calculated from Legendre polynomials fit to angular distribution data and is listed in Table I. The uncertainties shown in

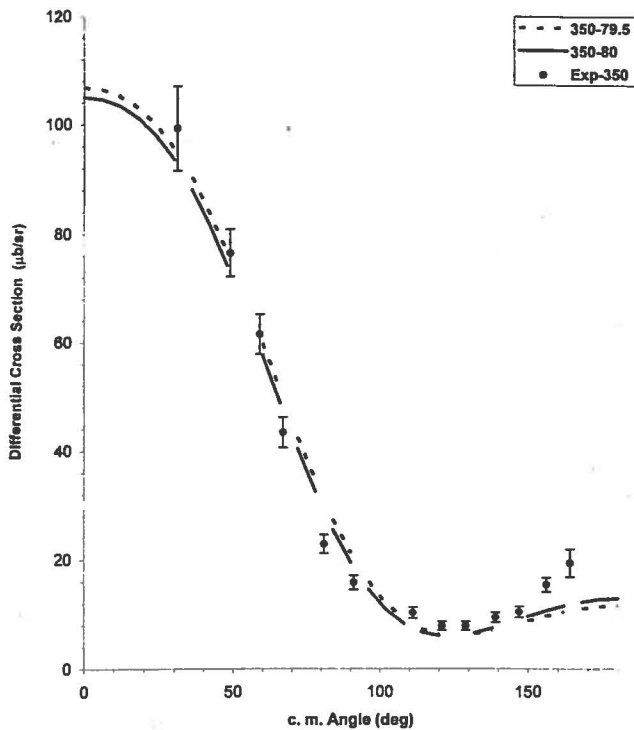


FIG. 3. Angular distributions of differential cross section for the  $^{13}\text{C}(d,p)^{14}\text{C}$  reaction at 350 keV deuteron energy. The dashed and solid curves are the results of finite range DWBA calculations using a real potential of 79.5 and 80 MeV, respectively.

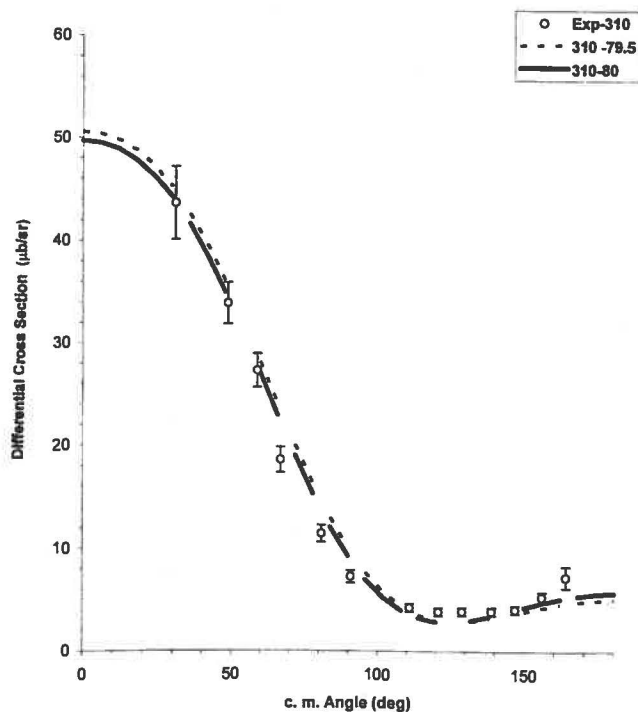


FIG. 4. Angular distributions of the differential cross for the  $^{13}\text{C}(d,p)^{14}\text{C}$  reaction at 310 keV deuteron energy. The dashed and solid curves are the results of the finite range DWBA calculations using a real potential of 79.5 and 80 MeV, respectively.

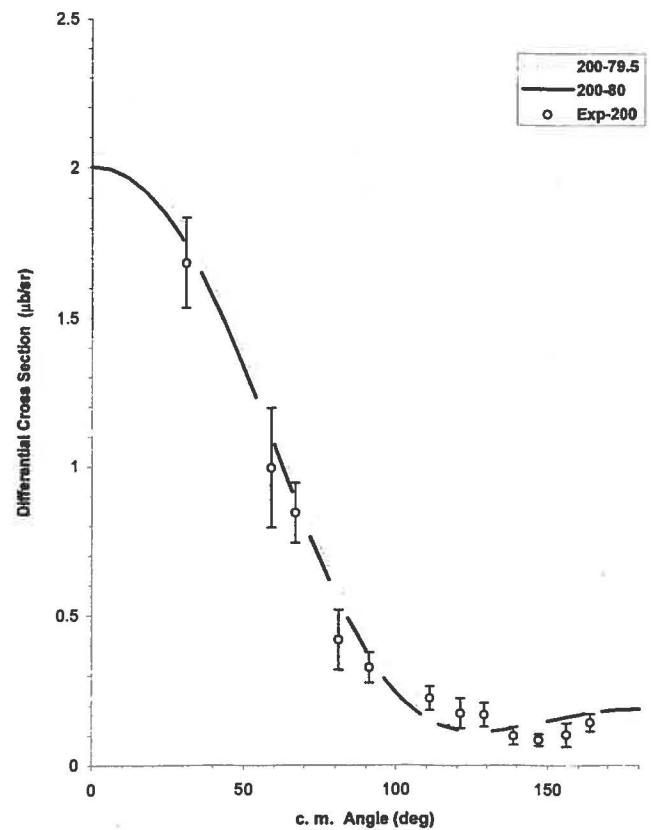


FIG. 5. Angular distributions of differential cross section for the  $^{13}\text{C}(d,p)^{14}\text{C}$  reaction at 200 keV deuteron energy. The dashed and solid curves are the results of finite range DWBA calculations using a real potential of 79.5 and 80 MeV, respectively.

the total cross section were calculated from uncertainty in values of coefficients of the Legendre polynomial fit.

### III. FINITE-RANGE DWBA ANALYSIS OF THE $^{13}\text{C}(d,p)^{14}\text{C}$ CROSS SECTION

The finite range DWBA model of direct reaction was used to analyze angular distribution data of the  $^{13}\text{C}(d,p)^{14}\text{C}$  reaction. The compound nucleus contribution in  $^{13}\text{C}(d,p)^{14}\text{C}$  reaction data at 200–350 keV deuteron energies were obtained from extrapolation of Putt's compound nucleus data [2] down to 200–350 keV deuteron energies. The estimated compound nucleus contributions at these deuteron energies were smaller than the experimental uncertainties in this data and therefore were ignored.

The finite-range DWBA calculations to fit  $^{13}\text{C}(d,p)^{14}\text{C}$  reaction cross section data were carried out using the finite-range DWBA code TWOFNR [9]. The code is a finite range version of a zero range DWBA code TWOSTP and it contains all the functions to calculate the finite-range form factor. The TWOSTP code was written to calculate differential scattering cross section for general form of the distorted wave Born approximation up to second order using the zero-range approximation. Therefore one-step and two-step processes of the reaction can be calculated using the TWOSTP program. For this code the incoming and outgoing waves may be in

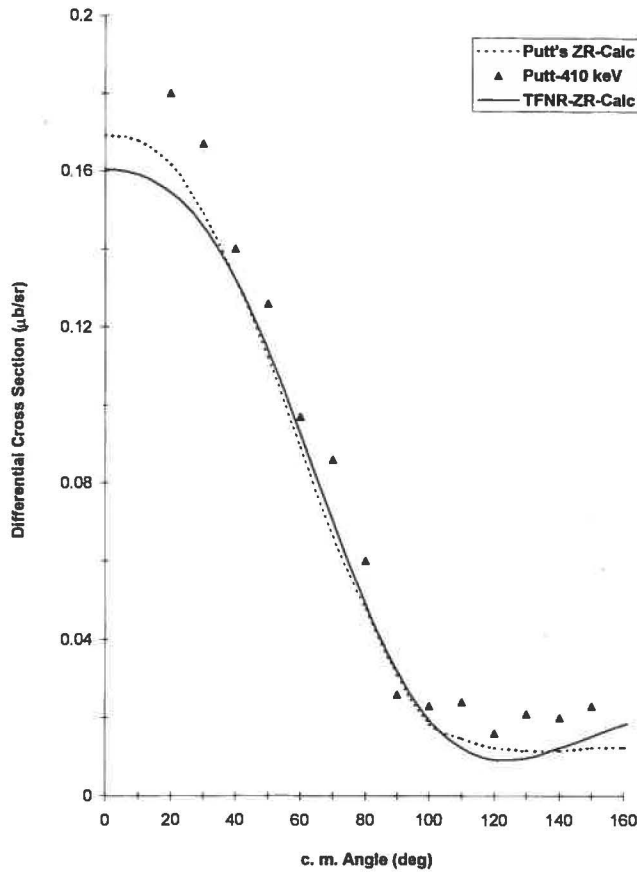


FIG. 6. Angular distributions of the differential cross section for the  $^{13}\text{C}(d,p)^{14}\text{C}$  reaction at 410 keV deuteron energy. The dashed and solid curves are the results of zero-range DWBA calculations by Putt and those obtained in this study by using the TWFNR code.

any combination of spin-0, spin- $\frac{1}{2}$ , or spin-1 particles. In the TWOSTP code, calculations are performed in a zero-range form factor between the coordinates of prior and post channels waves. The angular momentum algebra used in this program is almost similar to that of Satchler [10,11]. The TWFNR code has been successfully used in finite range DWBA analysis of transfer reaction data such as  $^{36,38}\text{Ar}(\bar{d},\alpha)^{34,36}\text{Cl}$  [12],  $^{58}\text{Ni}(\bar{d},\alpha)^{56}\text{Co}$  [13],  $^{31}\text{P}(\bar{d},^3\text{He})^{30}\text{Si}$  [14], and  $^{31}\text{P}(\bar{d},t)^{30}\text{P}$  [14]. In these calculations even  $D$ -state effects of triton and particles were also included. In very light nuclei  $D$  states are sensitive to details of the nucleon-nucleon tensor interaction.

In the present analysis of the  $^{13}\text{C}(d,p)^{14}\text{C}$  reaction cross section, finite range DWBA calculations were carried out using the TWFNR code. The wave functions of light and heavy bound systems were assumed to be of Wood-Saxon type. The depth of the binding potential for light and heavy bound systems were searched by the code for a given binding energy, potential radius, and diffuseness parameters. Values of potential depth were taken which reproduce correct binding energy for the light and heavy bound systems. For angular momentum transfer calculations the stripped neutron was assumed to be in the  $1s$  state and was captured in the  $1p$  state. The depth of the interaction potential was assumed to be the same as that of the light bound system.

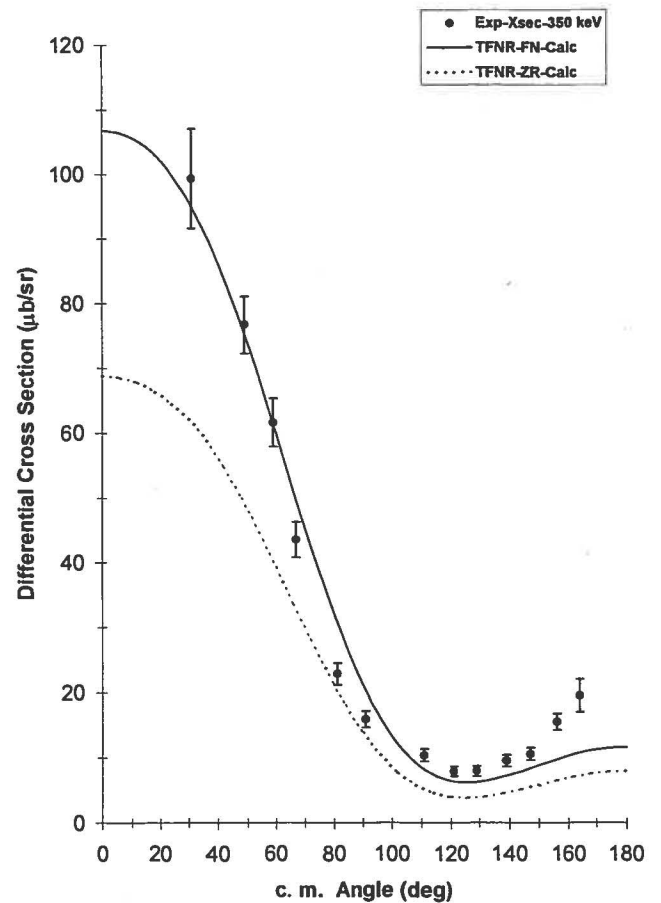


FIG. 7. Angular distributions of the differential cross section for the  $^{13}\text{C}(d,p)^{14}\text{C}$  reaction at 350 keV deuteron energy. The dashed and solid curves are the results of zero-range and finite-range DWBA calculations obtained in this study by using the TWFNR code.

The deuteron energies used in the present study were close to the 410–810 keV energy used by Putt [2]. Due to small energy difference between the present data set and Putt data set, it was assumed that present data can be analyzed using the same optical model parameters as used by Putt [2]. Also the value of the spectroscopic factor was taken from Ref. [2]. The finite-range DWBA analysis of the  $^{13}\text{C}(d,p)^{14}\text{C}$  reaction at 200–350 keV deuteron energies was carried out using the OMP parameters of Putt [2] data listed in Table II. The form of the potential used in this study with the TWFNR code is given by

$$U = -\{V_c f_c^{(R)}(r) + iW_c f_c^{(I)}(r)\} + 2\left(\frac{\hbar}{m_\pi c}\right)^2 \frac{1}{r} \frac{d}{dr} \\ \times \{V_{so} f_{so}^{(R)}(r)\} (\vec{l} \cdot \vec{s}) + \begin{cases} \frac{1}{2R_c} \left(3 - \frac{r^2}{R_c^2}\right) zZe^2, & r \leq R_c \\ \frac{1}{r} zZe^2, & r > R_c \end{cases}$$

where  $R$  and  $I$  are real and imaginary parts,  $V_c$ ,  $W_c$ , and  $V_{so}$  are the real, imaginary, and spin-orbit well depths of optical

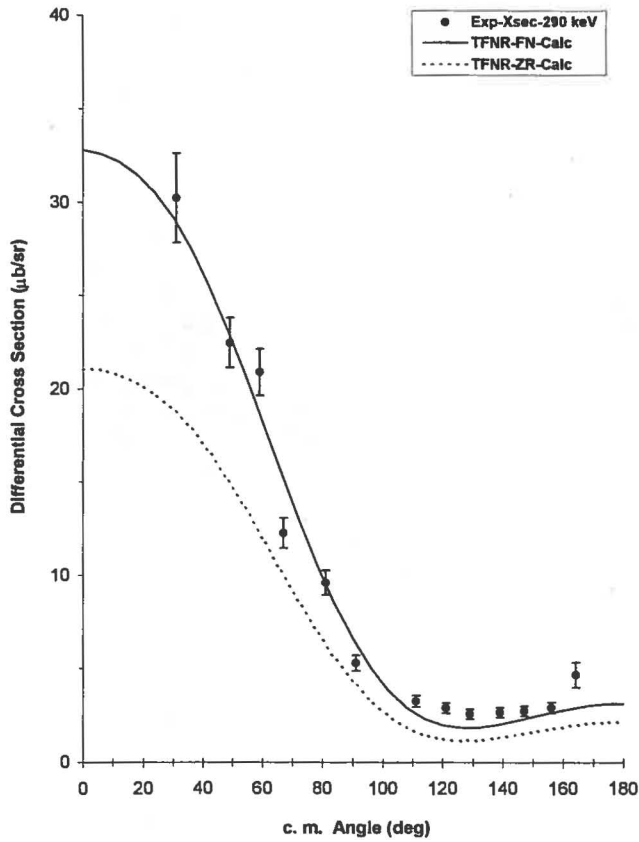


FIG. 8. Angular distributions of differential cross section for the  $^{13}\text{C}(d,p)^{14}\text{C}$  reaction at 290 keV deuteron energy. The dashed and solid curves are the results of zero-range and finite-range DWBA calculations obtained in this study by using the TWOFNR code.

potential,  $R$  and  $r$  are radius parameters, and  $R_c$  defines Coulomb radius. The  $f$ 's are associated form factors given as

$$f_c^{(R)}(r) = \frac{1}{1 + \exp[(r - R_R)/a_r]},$$

$$f_c^{(1)}(r) = (1 - C_{sd}) \frac{1}{1 + \exp[(r - R_1)/a_i]} + 4C_{sd} \exp\left(\frac{r - R_R}{a_i}\right) \frac{1}{1 + \exp[(r - R_1)/a_1]},$$

$$f_{so}^{(R)}(r) = \frac{1}{1 + \exp[(r - R_{SR})/a_{sr}]},$$

where

$$R_x = r_x m_T^{1/3}, \quad r_x > 0,$$

$$R_x = |r_x| (m_T^{1/3} + m_p^{1/3}), \quad r_x < 0.$$

$C_{sd}$  is the mixing factor of volume and surface imaginary wells.

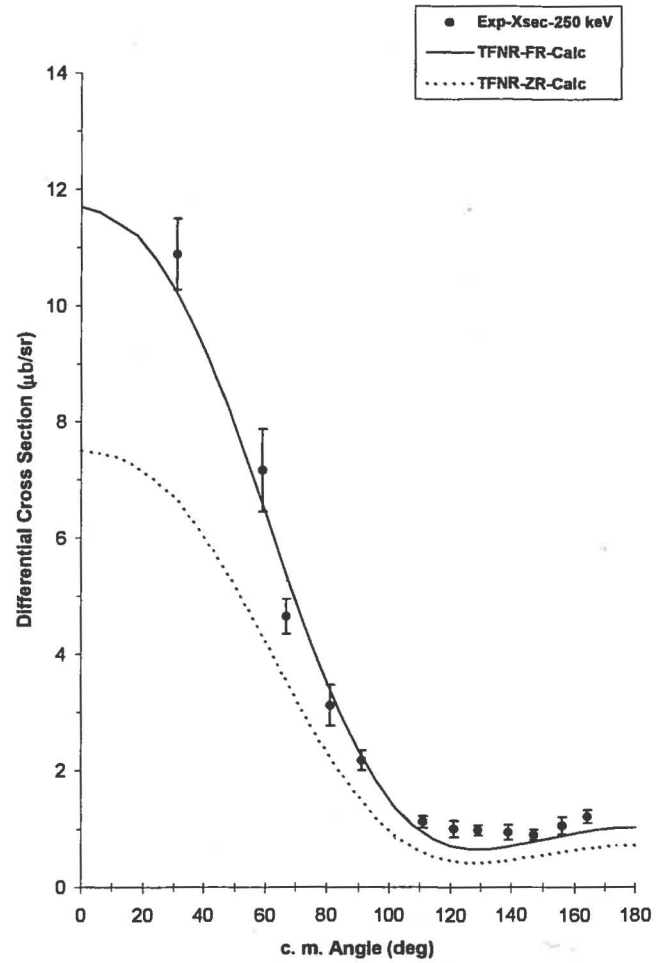


FIG. 9. Angular distributions of the differential cross section for the  $^{13}\text{C}(d,p)^{14}\text{C}$  reaction at 250 keV deuteron energy. The dashed and solid curves are the results of zero-range and finite-range DWBA calculations obtained in this study by using the TWOFNR code.

The angular distributions of the differential cross section as well as a total cross section was calculated for the  $^{13}\text{C}(d,p)^{14}\text{C}$  reaction at 200 to 350 keV deuteron energies using the finite range DWBA approximation. The total cross section is listed in Table I along with the experimental total cross section obtained in this study. Within statistical uncertainties, there is good agreement between the experimental and calculated total cross sections for the  $^{13}\text{C}(d,p)^{14}\text{C}$  reaction at 200–350 keV deuteron energies. Also

Figures 1 and 2 show experimental as well as calculated angular distributions of the differential cross section for the  $^{13}\text{C}(d,p)^{14}\text{C}$  reaction at 200 to 350 keV deuteron energies. There is good agreement between the calculated and experimental angular distributions at forward angles. At backward angles, i.e., angles greater than  $120^\circ$ , the DWBA model predicts a slightly lower cross section than the experimental cross section. Similar trends were also observed by Putt in the comparison of the normalized zero-range DWBA cross section calculations and the experimental differential cross sections for the  $^{13}\text{C}(d,p)^{14}\text{C}$  reaction at 410–810 keV deuteron energies [2].

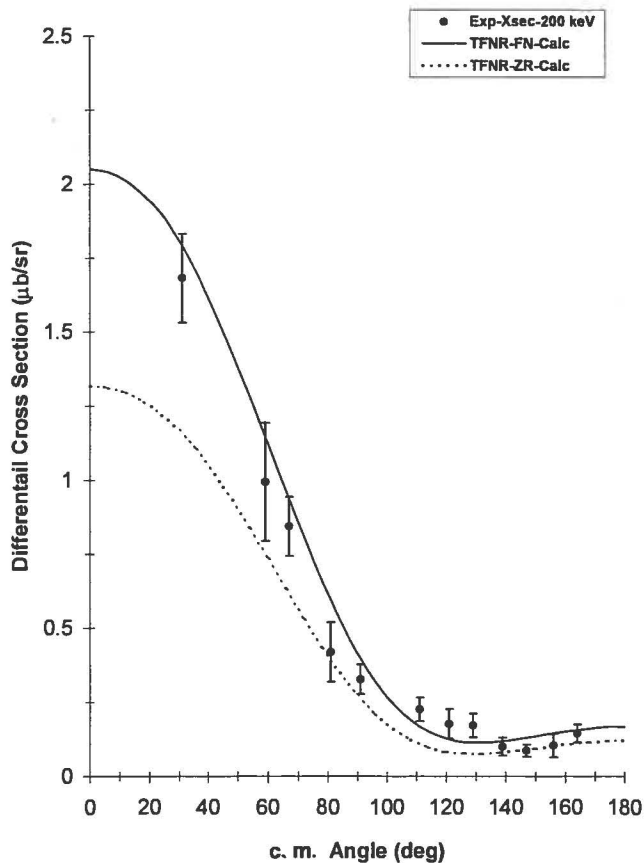


FIG. 10. Angular distributions of the differential cross section for the  $^{13}\text{C}(d,p)^{14}\text{C}$  reaction at 200 keV deuteron energy. The dashed and solid curves are the results of zero-range and finite-range DWBA calculations obtained in this study by using the TWOFNR code.

The angular distributions of the differential cross section for the  $^{13}\text{C}(d,p)^{14}\text{C}$  reaction calculated at the lower deuteron energy have better agreement with the experimental data. Furthermore if the depth of the real potential in the entrance channel is slight adjusted, even better agreement is achieved between the experimental and calculated angular distribution of the differential cross section for  $^{13}\text{C}(d,p)^{14}\text{C}$  reaction. An increase of 0.5 MeV in the depth of the real potential has improved the DWBA fit to experimental angular distributions over 200–350 keV deuteron energies, as shown in Fig. 3–5. The total cross section of the  $^{13}\text{C}(d,p)^{14}\text{C}$  reaction at 200 to 350 keV deuteron energies obtained in the DWBA calculations using  $V=80.0$  MeV is also listed in Table I along with  $\chi^2$  values. The calculated total cross section over 200 to 350 keV deuteron energies for  $V=80$  MeV still agree within statistical uncertainties with experimental values. The value of  $\chi^2$  has improved and it indicates a better fit to angular distribution. This is clearly shown in Figs. 3–5. For the sake of comparison, the DWBA fit to the angular distribution with  $V=79.5$  MeV has also been plotted in the Fig. 3–5.

The comparison of the two DWBA fits for  $V=79.5$  and  $V=80$  MeV to the experimental angular distribution of the  $^{13}\text{C}(d,p)^{14}\text{C}$  reaction at 350 keV, presented in Fig. 3 shows

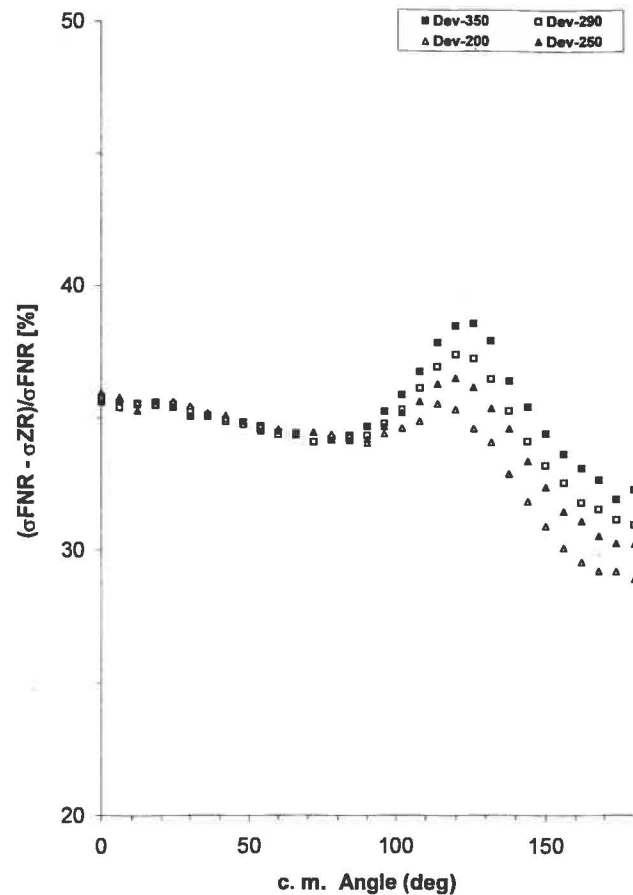


FIG. 11. Percentage deviation of the finite-range differential cross section from the zero-range differential cross section for the  $^{13}\text{C}(d,p)^{14}\text{C}$  reaction at 200–350 keV deuteron energy.

an improved fit to the experimental angular distribution at forward angles around  $60^\circ$ – $90^\circ$  as well as at backward angles around  $120^\circ$ – $150^\circ$ . The same is also true for Fig. 4 which show the two DWBA fits for  $V=79.5$  and  $V=80$  MeV to an experimental angular distribution of  $^{13}\text{C}(d,p)^{14}\text{C}$  reactions at 310 keV. Also there is an improvement in the DWBA fit to the experimental angular distribution at 200 keV for  $V=80$  MeV but only at forward angles. At backward angles, there is a better DWBA fit to the 200 keV angular distribution for  $V=79.5$ . This might be due to the decreasing direct reaction cross section at this energy and flattening of the angular distribution at backward angles.

#### IV. ZERO-RANGE DWBA ANALYSIS OF THE $^{13}\text{C}(d,p)^{14}\text{C}$ CROSS SECTION

It was stated earlier that zero-range DWBA calculations with a proper normalization constant may reproduce the results of a finite-range DWBA calculations [1]. Putt had calculated angular distributions of differential cross section for the  $^{13}\text{C}(d,p)^{14}\text{C}$  reaction at 410–810 keV deuteron energies and compared with the experimental data. He found a good agreement between the calculations and the experimental data using a normalization constant of 2.38. It was worth investigating that normalized zero-range DWBA calculations

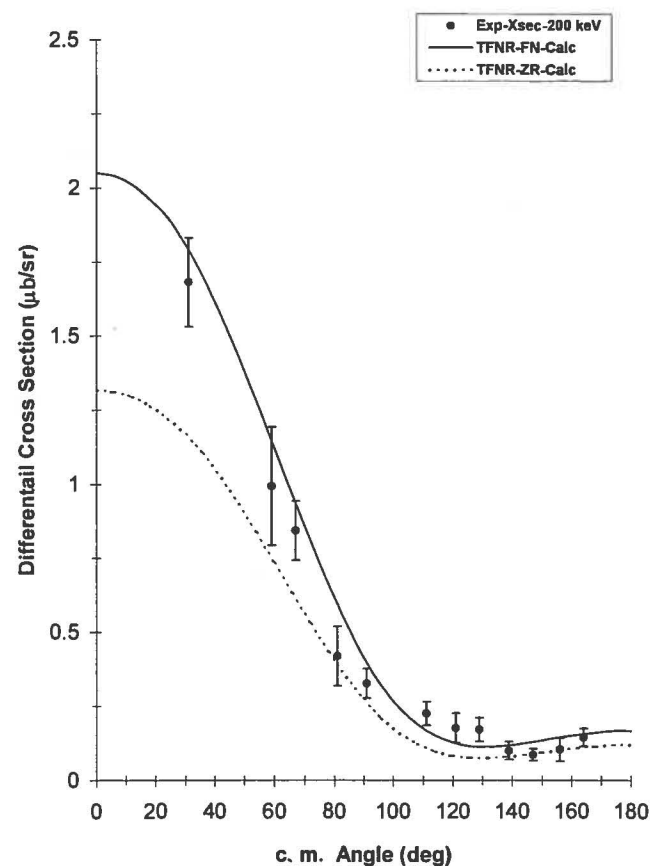


FIG. 10. Angular distributions of the differential cross section for the  $^{13}\text{C}(d,p)^{14}\text{C}$  reaction at 200 keV deuteron energy. The dashed and solid curves are the results of zero-range and finite-range DWBA calculations obtained in this study by using the TWOFNR code.

The angular distributions of the differential cross section for the  $^{13}\text{C}(d,p)^{14}\text{C}$  reaction calculated at the lower deuteron energy have better agreement with the experimental data. Furthermore if the depth of the real potential in the entrance channel is slight adjusted, even better agreement is achieved between the experimental and calculated angular distribution of the differential cross section for  $^{13}\text{C}(d,p)^{14}\text{C}$  reaction. An increase of 0.5 MeV in the depth of the real potential has improved the DWBA fit to experimental angular distributions over 200–350 keV deuteron energies, as shown in Fig. 3–5. The total cross section of the  $^{13}\text{C}(d,p)^{14}\text{C}$  reaction at 200 to 350 keV deuteron energies obtained in the DWBA calculations using  $V=80.0$  MeV is also listed in Table I along with  $\chi^2$  values. The calculated total cross section over 200 to 350 keV deuteron energies for  $V=80$  MeV still agree within statistical uncertainties with experimental values. The value of  $\chi^2$  has improved and it indicates a better fit to angular distribution. This is clearly shown in Figs. 3–5. For the sake of comparison, the DWBA fit to the angular distribution with  $V=79.5$  MeV has also been plotted in the Fig. 3–5.

The comparison of the two DWBA fits for  $V=79.5$  and  $V=80$  MeV to the experimental angular distribution of the  $^{13}\text{C}(d,p)^{14}\text{C}$  reaction at 350 keV, presented in Fig. 3 shows

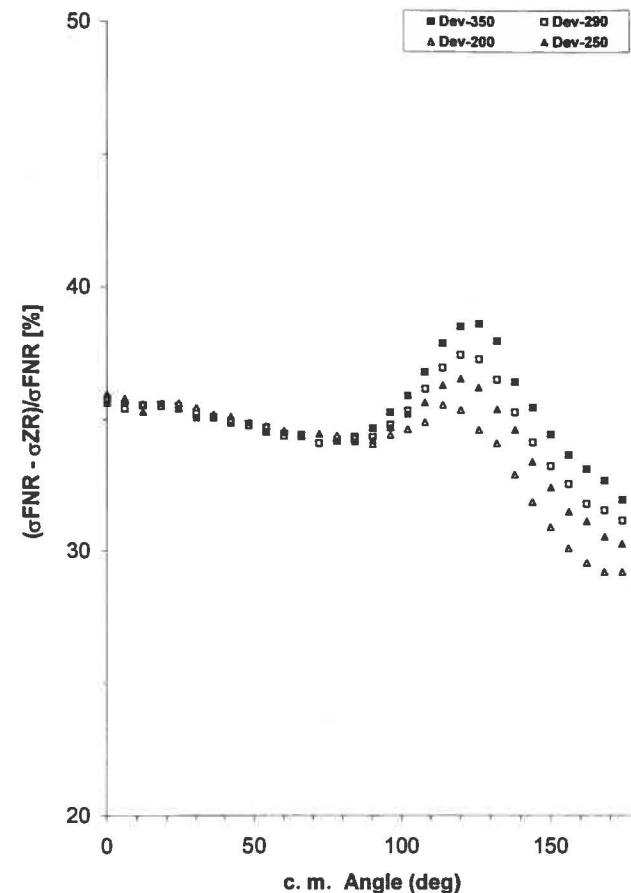


FIG. 11. Percentage deviation of the finite-range differential cross section from the zero-range differential cross section for the  $^{13}\text{C}(d,p)^{14}\text{C}$  reaction at 200–350 keV deuteron energy.

an improved fit to the experimental angular distribution at forward angles around  $60^\circ$ – $90^\circ$  as well as at backward angles around  $120^\circ$ – $150^\circ$ . The same is also true for Fig. 4 which show the two DWBA fits for  $V=79.5$  and  $V=80$  MeV to an experimental angular distribution of  $^{13}\text{C}(d,p)^{14}\text{C}$  reactions at 310 keV. Also there is an improvement in the DWBA fit to the experimental angular distribution at 200 keV for  $V=80$  MeV but only at forward angles. At backward angles, there is a better DWBA fit to the 200 keV angular distribution for  $V=79.5$ . This might be due to the decreasing direct reaction cross section at this energy and flattening of the angular distribution at backward angles.

#### IV. ZERO-RANGE DWBA ANALYSIS OF THE $^{13}\text{C}(d,p)^{14}\text{C}$ CROSS SECTION

It was stated earlier that zero-range DWBA calculations with a proper normalization constant may reproduce the results of a finite-range DWBA calculations [1]. Putt had calculated angular distributions of differential cross section for the  $^{13}\text{C}(d,p)^{14}\text{C}$  reaction at 410–810 keV deuteron energies and compared with the experimental data. He found a good agreement between the calculations and the experimental data using a normalization constant of 2.38. It was worth investigating that normalized zero-range DWBA calculations

may still fit angular distributions of differential cross section for  $^{13}\text{C}(d,p)^{14}\text{C}$  reaction measured at 200–350 keV deuteron energies.

For the reproducibility check, angular distributions of the differential cross section for the  $^{13}\text{C}(d,p)^{14}\text{C}$  reaction was calculated at 410 keV deuteron energy using the TWOFNR code and was compared with the zero-range calculations of Putt. With a normalization constant of 2.38, the results of a zero-range calculation by TWOFNR is in good agreement with the zero-range calculations of Putt. This is clearly shown in Fig. 6. Then angular distributions of the differential cross section for the  $^{13}\text{C}(d,p)^{14}\text{C}$  reaction were calculated at 200–350 keV deuteron energies using a zero-range DWBA approximation. The results of these calculations at 200, 250, 290, and 350 keV deuteron energies are shown in Figs. 7–10. Angular distributions of differential cross sections for the  $^{13}\text{C}(d,p)^{14}\text{C}$  reaction generated by the finite range calculations are also superimposed on the zero-range calculation results. A comparison of finite-range and zero-range cross section data at 200, 250, 290, and 350 keV deuteron energies show that the zero-range calculations underestimates the differential cross section at all angles by energies. Figure 11 shows the percentage deviation of a zero-range cross section from the finite range cross section for the  $^{13}\text{C}(d,p)^{14}\text{C}$  reaction as a function of c.m. angles at 200, 250, 290, and 350 keV deuteron energy. Below the  $100^\circ$  c.m. angle there is a constant deviation but at angles larger than  $100^\circ$  the deviation

varies between 30–40 % depending upon the deuteron energy. This larger deviation at backward angles is due to a change in angular distribution shape at backward angles for a finite range calculation at higher deuteron energies.

#### V. CONCLUSION

The results of the present study has provided a finite-range DWBA fit to  $^{13}\text{C}(d,p)^{14}\text{C}$  cross section data at 200–350 keV deuteron energies. The good agreement between the experimental data and the calculations indicates that the high  $Q$  value  $^{13}\text{C}(d,p)^{14}\text{C}$  reactions at  $E_d=200$ – $350$  keV energy can still be described quantitatively by the finite-range DWBA model. For the sake of comparison, the angular distribution of the differential cross section for the  $^{13}\text{C}(d,p)^{14}\text{C}$  reaction at 200, 250, 290, and 350 keV deuteron energies were also calculated using the zero-range DWBA approximation. It was observed that the zero-range calculation underestimates the cross section at all angles by 30–40 % over 200–350 keV deuterons energy range.

#### ACKNOWLEDGMENTS

The authors wish to acknowledge the support of the Research Institute of King Fahd University of Petroleum & Minerals, Dhahran, Saudi Arabia.

- [1] M. M. Nagadi, A. A. Naqvi, S. Kidwai, M. A. Al-Ohali, and F. Z. Khiari, *Aust. J. Phys.* **51**, 913 (1998).
- [2] G. D. Putt, *Nucl. Phys.* **A161**, 547 (1971).
- [3] L. L. Lee, Jr., J. P. Schiffer, B. Zeidman, G. R. Satchler, R. D. Drisko, and R. H. Basel, *Phys. Rev.* **136**, B971 (1964).
- [4] G. R. Satchler, *Nucl. Phys.* **55**, 1 (1964).
- [5] N. Austern, R. M. Drisko, E. C. Halbert, and G. R. Satchler, *Phys. Rev.* **133**, B3 (1964).
- [6] A. A. Naqvi, Abdulaziz A. Al-Jalal, A. Coban, and F. Z. Khiari, *Nuovo Cimento A* **105**, 1501 (1992).
- [7] A. A. Naqvi, M. M. Nagadi, S. Kidwai, M. A. Al-Ohali, and F. Z. Khiari, *Aust. J. Phys.* **51**, 903 (1998).
- [8] M. Al-Jalal, A. A. Naqvi, H. A. Al-Juwair, A. Coban, and F. Z. Khiari, *Arabian J. Sci. Eng.* **20**, 179 (1995).
- [9] TWOFNR, User Manual: URL <http://www.tac.tsukuba.ac.jp/~yaoki/twofnr.pdf>
- [10] G. R. Satchler, *Nucl. Phys.* **55**, 1 (1964).
- [11] G. R. Satchler, *Lectures in Theoretical Physics, Vol. VIII C, Nuclear Structure Physics*, edited by P. D. Kunze *et al.* (The University of Colorado Press, Boulder, 1966), pp. 73–110.
- [12] C. M. Bhat, Y. Tagishi, E. J. Ludwig, and B. A. Brown, *Phys. Rev. C* **34**, 736 (1986).
- [13] E. R. Crosson, R. K. Das, S. K. Lemieux, E. J. Ludwig, W. J. Thompson, M. Bisenberger, R. Hertenberger, D. Hofer, H. Hofer, H. Kader, P. Schiemenz, G. Graw, A. M. Eiro, and F. D. Santos, *Phys. Rev. C* **45**, R492 (1992).
- [14] C. M. Bhat, J. E. Bowsher, T. B. Clegg, H. J. Karowski, E. J. Ludwig, and B. A. Brown, *Phys. Rev. C* **38**, 1537 (1988).